Determination of the Creep Properties of Pb-free Solders for Harsh Environments Using Meso-scale Testing

S. Godard Desmarest, C. Johnston and P. S. Grant
University of Oxford, Department of Materials

Parks Road, Oxford, OX1 3PH, UK
Tel. +00 44 (0) 1865 283 707
sophie.godarddesmarest@materials.ox.ac.uk

Abstract

Solder joints in electronic packages are prone to failure due to the evolution of thermal expansion mismatch strains during thermal cycling. The comparatively wide operating temperature range and long lifetimes of aerospace electronics require high reliability solder joints. Since 2006, high reliability industries (aerospace and military amongst others) that are exempt from lead-free RoHS regulation on account of concerns over the reliability of Pb-free solders have found it increasingly difficult and expensive to continue using traditional Sn-Pb-based solders. Hence there is a pressing need to find a suitable alternative that can match the manufacturing and reliability performance of Sn-Pb. There remains a dearth of data for the constitutive behaviour of Pb-free solders under harsh environment scenarios. Unfortunately, conventional test approaches, particularly in the case of creep behaviour which is critical to solder lifetimes, are expensive and time-consuming. High temperature nanoindentation has been recently developed as a quick method for the determination of creep properties of solder alloys. This paper compares and contrasts nanoindentation creep results for bulk Pb-Sn and lead-free solders. However, there are limits to nanoindentation creep, in particular the load-dependence of the technique. A new meso-scale test approach that lies between nanoindentation and bulk creep testing has been developed. Real ball grid arrays using Pb-free solders have been creep tested in the temperature and stress ranges of operating solder joints. High temperature creep constitutive data has been obtained. The technique offers promising time and materials savings in obtaining important mechanical property data for subsequent use in life-prediction models.

Keywords: Pb-free solder, creep, harsh environments, Nanoindentation

1 Introduction

Since July 2006, the worldwide electronic industry supply chain has moved to Pb-free in electronic assemblies because of the implementation of the European Union RoHS (Restriction of Hazardous Substances in Electrical and Electronic Equipment) [1] directive that bans the use of Pb in most electronics. Since 2000, the industry has converged towards the near eutectic ternary Sn-Ag-Cu (SAC) solder system, now considered the most suited to replace Sn-Pb solder because SAC solders exhibit better mechanical properties than Sn-Pb solders (in particular strength, elongation, creep and fatigue resistance). Although there is still no drop-in replacement alloy to eutectic Sn-Pb, most of the solders in surface mount assemblies have compositions containing 3.0-4.0 wt% Ag and 0.5-0.9 wt% Cu, with the remainder Sn. All alloy compositions will hereafter be expressed as Sn-xX-yY, where X and Y are alloying elements in Sn, with the composition being x mass fraction *100 of element X, y mass fraction *100 of element Y and remainder being Sn.

Although the RoHS legislation only applies to products on the European market, almost all global manufacturers have moved to Pb-free as it is uneconomical to produce both RoHS-compliant and non-RoHS-compliant electronic assemblies in parallel. However, high reliability industries (aerospace, military, subsea and maritime, instruments for down-hole applications, power generation and power distribution) are exempt from this regulation because of concerns over the reliability of Pb-free solders in harsh environments. The reliability of electronic assemblies for such applications is very often critical and the key components of electronic assemblies are the solder joints. The electronics of these industries must be able to withstand an extended thermal range (-55 to 125°C) and longer life-times

(up to 40 years) than domestic electronics (3-5 years). Such conditions degrade more rapidly reliability and life-times of electronic assemblies.

However, a valid quantification of the loss of reliability for harsh environment Pb-free electronics remains unknown. While traditional eutectic Sn-37Pb has been used for over fifty years with well-known time to failure knowledge and reliable life-time prediction models for the different assembly types, Pb-free solders do not have such a legacy of performance data. Harsh environment industries account for a marginal share of the world electronic equipment production (8% for the automotive industry, 7% for the aerospace and defence industry [2]) and find it increasingly difficult and expensive to continue using Sn-Pb-based electronics. Besides, there have been reports that a RoHS2 directive will soon expand the RoHS scope to all electrical and electronic equipment sold in the European Union, including the currently exempted industries. Hence there is a pressing need to find a suitable alternative that can match the manufacturing and reliability performance of Sn-Pb.

In order to validate a new solder material, extensive cyclic thermal testing has to be carried out to evaluate material behaviour under realistic operating conditions. Numerical models are commonly used to speed up this process and to compare various assembly designs. Accurate life-time predictions require a full understanding of failure modes as well as an experimental reliability database to calibrate life-prediction models. One of the main criterion for reliable estimation of real life behaviour of electronics is the accuracy of the materials parameters inserted in the model. However, gaining this critical data by mechanical testing is a long-winded process. Traditionally, new solders are firstly tested in bulk for weeks in tensile test machines to characterise their mechanical properties. This is a long and expensive process. Nanoindentation is a powerful tool to characterise quickly the mechanical behaviour of solder alloys at room temperatures. Recently, high temperature nanoindentation has offered exciting developments for the characterisation of solder creep properties. However bulk material and solder joint microstructures differ due to different processing conditions. Concerns over the load-dependence of nanoindentation may arise. Besides, the stress range of nanoindentation tests is much higher than the operating conditions (1 to 10 MPa). A novel method that will speed up mechanical characterisation and that will provide crucial data for the development of new Pb-free solder materials for harsh environment applications is described.

2 Objectives

- To provide the first elevated temperature nanoindentation creep study on a range of various solder materials.
- To evaluate the validity of elevated temperature nanoindentation for the characterisation of solder creep properties by comparison with conventional tensile testing results.
- To compare traditional Sn-37Pb alloys with Pb-free solders by means of comprehensive microstructural analysis.
- To describe a novel method that would allow for high temperature shear testing of entire solder joints.
- To provide preliminary data for this new meso-scale test and compare with traditional testing.

3 Creep in Solder Alloys

In electronic assemblies, failures arise as solder joints relax thermal stresses through creep and fatigue mechanisms. In service, microelectronic solder joints undergo thermal cycling, due to both the environment and operation. The different response of the various parts of the assembly to temperature cycles due to thermal expansion mismatch results in low-cycle fatigue. The board may shrink (Figure 1*a*, *b*) or expand, resulting in mechanical stresses in solder joints. Solders accommodate cyclic strains until eventual failure (Figure 1*c*). Creep dominates the deformation kinetics in joints as they operate at a high homologous temperature.

The creep behaviour of solder alloys can be studied by various techniques such as conventional tensile creep, [4] uniaxial tensile, [5] stress relaxation, [6] impression, [7, 8] and indentation tests. Time-dependent properties such as creep have been studied by various indentation experiments including hot-hardness tests, [9] room temperature Vickers indentation, room temperature nanoindentation. [10] Although the most widely used method is the conventional tensile creep test, indentation techniques offer a promising time-saving alternative method. [11] Recently, elevated temperature nanoindentation has been considered a possible very powerful technique to obtain quickly properties of materials,

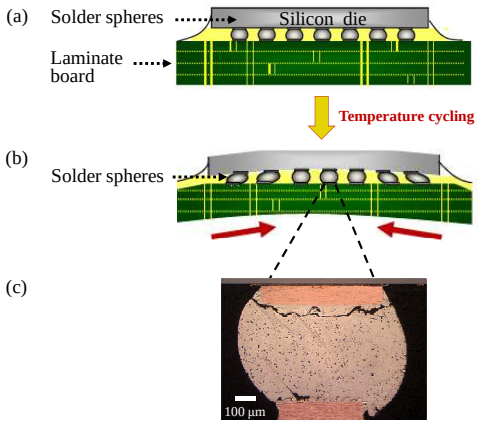

Figure 1: ***a*** **Schematic of a ball grid array (BGA), type of surface mount technology (SMT) electronic package, showing the chip, the PCB and the array of solder balls, with typical dimensions;** ***b*** **optical micrograph of failure in a SAC387 ($SnAg_{3.8}Cu_{0.7}$) ball-grid-array (BGA) electronic package due to thermal cycling at 0-100°C. [3]**

in particular creep properties. [12] Creep parameters in standard steady-state such as stress exponents n and creep activation energies Q can be obtained by best fit to data obtained from creep experiments. Stress exponents values are associated with different deformation mechanisms. High temperature nanoindentation has been steadily improved since the first high temperature nanoindentation measurement carried out in 1995 by placing the nanoindenter in a temperature-controlled room up to 32-34°C. [13] High temperature nanoindentation now enables recording of indentation load and penetration depth during indentation process at temperatures up to 750°C. However, only few attempts have been made to compare creep results from conventional creep tests with indentation on the same material. There has been very limited work on the elevated temperature nanoindentation of solder alloys. [12]

4 Nanoindentation

4.1 Materials

Bulk eutectic Sn-37Pb, SAC387 and Innolot from wave soldering bars as well as a bulk Sn sample with a 99.99% purity and grain size $\geq$ 10 μm were studied. Innolot is a promising new solder specifically designed for the automotive industry and produced by Cookson Electronics. Its composition is $SnAg_{3.8}Cu_{0.7}Bi_{3.0}Sb_{1.0}$, developed on the basis of SAC387. Innolot had improved reliability compared with SAC387 in both vibration testing after zero and 500 thermal cycles and thermal cycling in the -40°C to +150°C temperature range. [14] Samples were ground with 600, 1200, 2500 and 4000 SiC paper, then carefully polished with 1 and 0.25 μm diamond suspensions and then finished and slightly etched in a 0.06 μm colloidal silica suspension.

While Sn-37Pb was constituted of Pb islands embedded in a Sn matrix, the microstructure of SAC387 and Innolot consisted of small intermetallic particles of Cu_6Sn_5 and Ag_3Sn embedded in Sn matrix (Figure 2). The various phases were identified by a combination of morphology and Energy Dispersive X-ray analysis (EDX). Innolot contained impurities of Bi and Sb particles in a predominantly β-Sn-rich matrix as well as $(Cu,Ni)_6Sn_5$ and Ag_3Sn intermetallics.

4.2 Experimental Methods

Experiments were performed using a NanoTest platform supplied by Micro Materials Ltd., Wrexham, UK. Nanoindentation used a pendulum-mounted indenter with electromagnetic loading and parallel plate capacitors for depth measurement. During nanoindentation, the penetration depth of a calibrated Berkovich indenter was measured as a function of the applied load throughout a load-unload cycle. Experiments consisted of constant loading rate indentation cycles, with loading to various maximum loads at 6.66 $mN.s^{-1}$ followed by a 600 s dwell at maximum load, unloading at 6.66 $mN.s^{-1}$ and a second dwell period of 15s at 90% unloading for thermal drift corrections. Prior to measurements, the compliance of the loading frame was accounted for by performing high load indents into fused silica. Geometry corrections from the ideal Berkovich indenter were made by placing indents in fused silica over a range of depths for each temperature prior to measurements.

Figure 3 shows typical load-depth curves obtained for SAC387 solder alloys at 25, 50, 100, 150 and 175°C. Higher testing temperatures with constant loading rate led to faster indenter penetration, significant of the softening of the materials with temperature increase. Creep was observed during the dwell periods at maximum load.

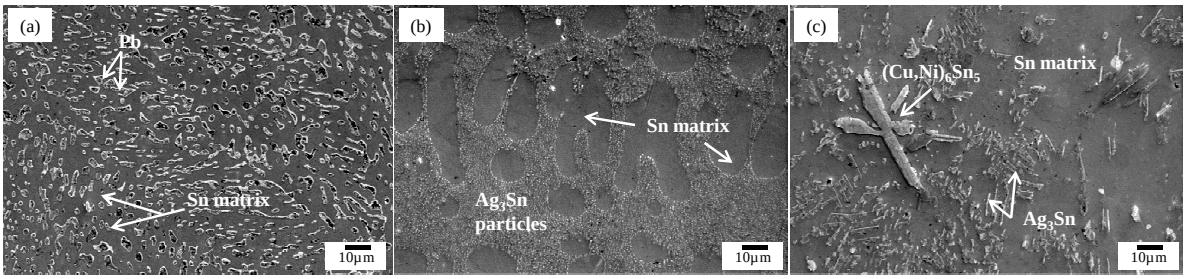

Figure 2: Scanning Electron Microscope (SEM) picture of bulk *(a)* eutectic Sn-37Pb; *(b)* SAC387 and *(c)* Innolot.

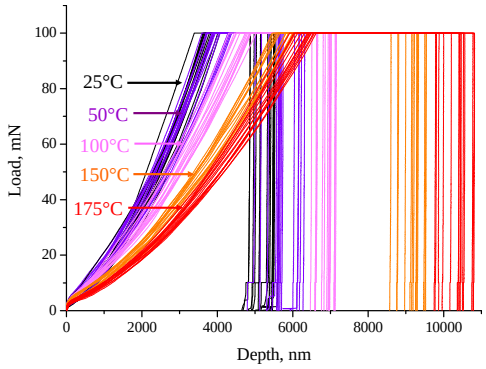

Figure 3: Indentation load-depth curves of SAC387 at 25, 50, 100, 150 and 175°C.

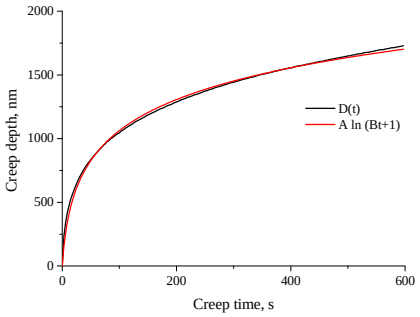

Figure 4: Experimental creep curve on bulk SAC387 at 25°C and the best fit to Equation 1. All alloys showed similar exponential behaviour and accordance to Equation 1.

4.3 Nanoindentation Creep Results and Discussion

4.3.1 Determination of Creep Stress Exponents

The initial phase of nanoindentation creep was fitted to the Chudoba and Richter equation (Figure 4): [15]

$$D(t) - D(0) = A ln(Bt + 1) \quad (1)$$

where $D(t)$ is the indentation depth (nm), t is the creep time (s) and A and B are material constants that can be related to the extent of creep and the creeping rate, respectively.

It was assumed that the creep deformation of the alloys was due to steady-state creep and that the creep data could be best-fitted to the secondary creep equation, also called Dorn power law equation:

$$\frac{d\epsilon_s}{dt} = B\sigma^n exp\left(-\frac{Q}{RT}\right) \quad (2)$$

where $\frac{d\epsilon_s}{dt}$ is the steady-state creep strain rate, B and n are constants, Q is the activation energy for the creep process and R is the universal gas constant. The creep strain rate $\frac{d\epsilon}{dt}$ was:

$$\frac{d\epsilon}{dt} = \frac{1}{h}\frac{dh}{dt} \quad (3)$$

where h is the indentation depth. Although the stress around an indent varies greatly between the indentation area and more remote regions, a characteristic stress σ can be defined by a relationship similar to the hardness definition [16]:

$$\sigma = \frac{P}{A_p} \quad (4)$$

where P is the applied load and A_p is the cross-sectional area of the indenter. Experimental creep parameters can be extracted from nanoindentation creep studies at constant load by combining Equations (2)-(4) [16]:

$$ln\left(\frac{1}{h}\frac{dh}{dt}\right) = lnk + nln\left(\frac{P}{A}\right) \quad (5)$$

where k is a constant.

The stress exponent n was extracted from the linear best-fit regression using a log-log plot of $\frac{1}{h}\frac{dh}{dt}$ against $\frac{P}{A}$.

Figures 5 and 6 show the creep curves obtained for bulk SAC387, Sn, Sn-37Pb and Innolot at 25 and 150°C and stress exponents data determined by high temperature nanoindentation creep at 100 mN in the 25-175°C temperature range.

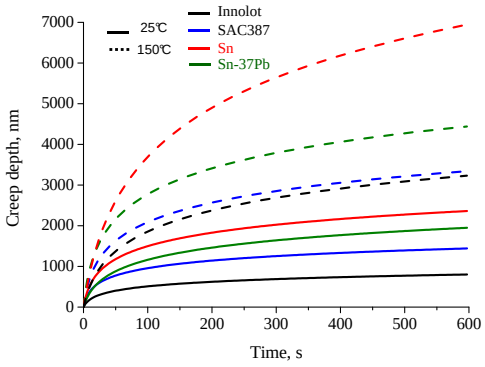

Figure 5: Creep curves obtained for bulk Innolot, SAC387, Sn, Sn-37Pb at 25 and 150°C, under a 100 mN load for 600 s

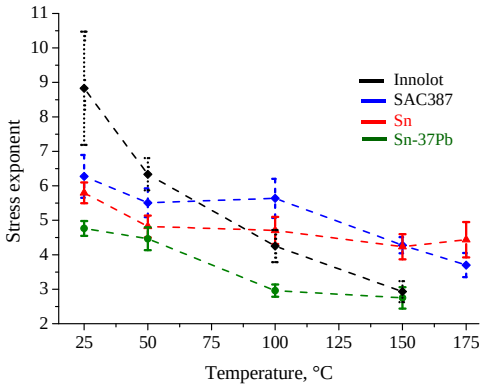

Figure 6: Stress exponent values for bulk SAC387, Sn, Sn-37Pb and Innolot as a function of temperature at 100 mN.

There was an overall decrease of the stress exponents with temperature. The creep exponent decreased from 8.8, 6.3, 5.8 and 4.8 at 25°C to 2.9, 3.7, 4.2 and 2.8 at 150°C for Innolot, SAC387, Sn and Sn-37Pb, respectively. The decrease was therefore of 67, 41, 28 and 42% for Innolot, SAC387, Sn and Sn-37Pb, respectively. According to Equation 2, a decrease in the stress exponent results in an increase in creep rate, which can be linked to a decrease in yield strength. Therefore, the lower the stress exponent value, the less creep resistant the alloy is. At 25°C, Figures 6 and 5 showed $n_{Sn} < n_{SnPb} < n_{SAC387} < n_{Innolot}$, which was in accordance with the strengthening effect of intermetallics. For Innnolot, the presence of Bi and Sb and the presence of $(Cu,Ni)_6Sn_5$ intermetallics in the microstructure resulted in the two alloying mechanisms of solid solution strengthening and dispersion hardening, hence the higher creep resistance of Innolot and SAC387 solders compared to Sn and Sn-37Pb. The decrease of the stress exponent values with temperature increase is characteristic of the softening effects and the thermal activation of creep. Figure 6) showed two distinct regions, for T<50°C and T>100°C, suggesting two separate mechanisms. Grain boundary sliding at low temperature followed by viscous flow at high temperatures for Sn-37Pb, Sn, SAC387 and Innolot solder alloys. In SAC387 and Innolot, the intermetallics trap and pin dislocations, impeding their movement, thus slowing down the grain boundary sliding mechanism. Therefore, grain boundary sliding is expected to dominate first in Pb-free solders, followed by dislocation climb.

Innolot differed from other alloys by a dramatic drop in the stress exponent values of about 67% that led to $n_{SAC387} > n_{Innolot}$ at 150°C. Figure 5 showed almost the same creep behaviour for SAC387 and Innolot, thus the creep strain rate of Innolot was similar to that of SAC387 at 150°C. It was the increase of the projected contact area with temperature which was much larger for Innolot than for SAC387. Therefore, the strengthening effect of intermetallics in Innolot was very much decreased by a temperature increase, which raises concern over the suitability of Innolot for high temperature applications of electronic assemblies. Besides, not only does the strengthening effect of intermetallics decreased at high temperatures, it also rendered Innolot more brittle (Figure 7).

The apparent brittleness of Innolot was counterbalanced by the fact that intermetallics were evidenced to stop crack propagation (Figure 8*b*). In Sn-Pb, the Pb islands acted as crack initiators around the indent site and cracks propagated from one Pb island to the closest, reaching a propagation length of 100μm in the bulk for a 200 mN indent (Figure 8*a*).

4.3.2 Determination of Creep Activation Energies

Figure 9 *(a)* and *(b)* shows a schematic description of how the creep activation energy Q can be determined [11]. At a given temperature, Equation 2 gives Q as the slope of the *ln (strain rate)* against *1/T*. The strain rate is calculated from the median of the creep curves measured at a particular temperatures and fitted to Equation 1. Figure 10 gives the best-fit values of Q determined at an indenter depth of 1.3 μm.

The calculated values were 34.6, 30.1, 24.6 and 20.4 kJ.mol^{-1} for Innolot, Sn-37Pb, SAC387 and Sn, respectively. Values of stress exponents obtained at room temperature and activation energies were included in 1. Creep testing showed good agreement between impression creep tests and conventional creep

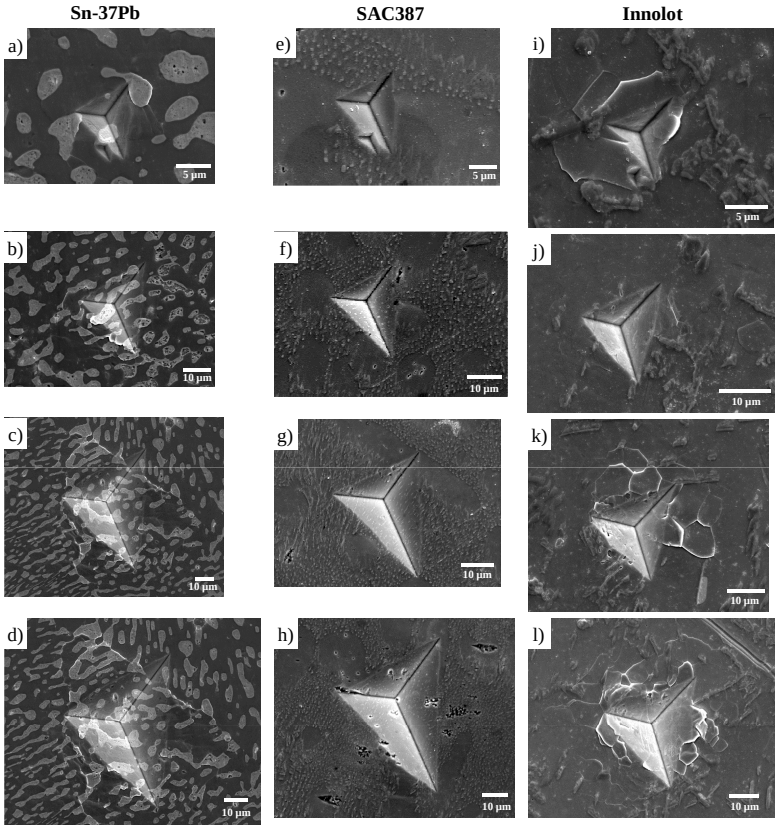

Figure 7: SEM picture of indents on eutectic Sn-37Pb, SAC387 and Innolot for loads of 10, 50, 100 and 200 mN (*a)* to *d)*, *e)* to *h)* and *i)* to *l)*), respectively. Sn-Pb showed little cracking from 10 to 200 mN. No cracking was observed for SAC387, indicating that at these loads, the solder could plastically deform without fracturing. Extensive cracking was observed on Innolot at all loads.

tests [17]. Comparison of nanoindentation with conventional testing results was not straightforward. There was large discrepancies between various studies, even amongst similar conventional tests.

4.4 Comparison between Nanoindentation and Conventional Tensile Tests Results

Discrepancies amongst research studies can be primarily attributed to differences in sample preparation and experimental techniques. The microstuctural difference between bulk tensile tested samples and nanoindented samples might explain the deviation between studies. In particular, the grain size dependence of creep mechanisms may be highlighted. [16,18]

However, the validity of the assumptions made for the interpretation of nanoindentation creep may also be questioned. Recently, room temperature nanoindentation as a method to obtain bulk creep properties was assessed as being 'uncertain'on a range of materials because of its poor reproducibility. [11]

In nanoindentation, the creep rate at constant load eventually slows to zero because the volume of creeping material increases as the indenter penetration increases until the load becomes too small to promote any appreciable creep. Little mention of the fact that Equation 2 does not take into account the lowering stress during depth increase (due to the increase of the contact area) was found in the literature. [15] In case of load-dependence of nanoindentation creep, the relevance of the data obtained above can be questioned. Previous study on Pb-1.25Sb and Pb-4.5Sb has shown that stress exponent values are independent of the loading conditions in hardness tests [28]. Impression creep on Sn-Pb were strongly stress-dependent on the activation energy [17]. The stress dependence seems to be better taken into account by the Garofalo model (Equation 6), than the Dorn power law (Equation 2).

$$\frac{d\epsilon_s}{dt} = C\,[sinh(\alpha\sigma)]^{n'} exp\,(-\frac{Q'}{kT}) \qquad (6)$$

where α is the stress coefficient that prescribes the stress level at which the power law dependence breaks down (in MPa), Q' is the activa-

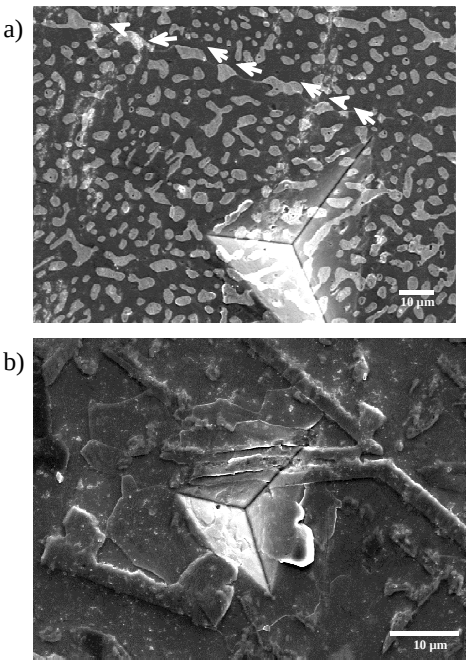

Figure 8: SEM picture of indentation induced cracking for *a)* Eutectic Sn-37Pb (200 mN load) and *b)* Innolot (100 mN load)

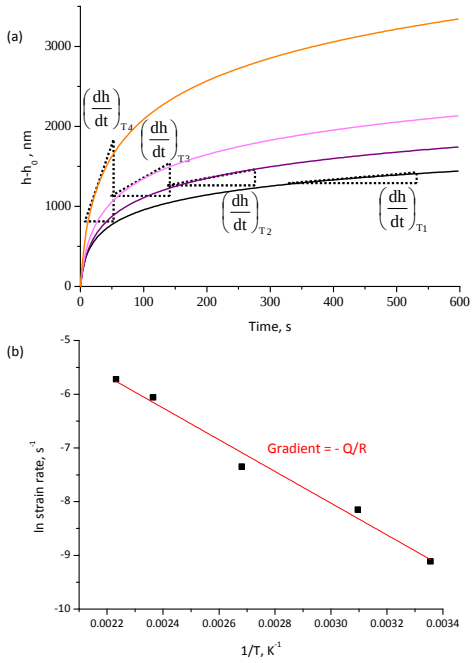

Figure 9: (b) Determination of the SAC387 creep activation energy *Q*, from (a) elevated temperature creep curves of SAC387.

tion energy and *C* is a constant. In Juhasz's study on Sn-Pb [17], the activation energy obtained in the superplastic region by impression creep was 40 to 45 kJ.mol$_1$, in good agreement with tensile measurements. When stresses decrease, the work necessary to overcome obstacles is increasingly controlled by the thermal processes, at the expense of mechanical work. Impression creep on Sn-Pb eutectic alloys showed stress exponent increase with stress from 1 to 3.5 for temperature ranging from 80 to 110°C and 2.5 to 6 within the 25 to 65°C range [29]. The stress dependence obeyed a Garofalo hyperbolic sine type function of stress for all the ranges of stresses and temperatures. Similarly, the activation energy was found to increase abnormally with stress. Using the hyperbolic sine function, a single activation energy of 55 kJ.mol^{-1} was found. Therefore, the choice of the model for the interpretation of indentation creep data is critical. It is also critical for creep results obtained from tensile tests, as outlined in Table 1, which shows the creep parameters obtained for the Dorn power law and the Garofalo hyperbolic sine law models, respectively, for a range of solder alloys.

Another questionable hypothesis for nanoindentation creep is the steady-state condition since strain rates in the primary creep region are much higher under the same loading conditions than strain rates in conventional creep testing. However, good agreement between nanoindentation and bulk for Sn-38Pb has been found [16] and suggests that, for a high creeping material, a reasonable agreement can be expected as the high secondary creep rates reduces the effect of primary creep. Moreover, elevated temperature nanoindentation, which gives higher creep rates still, should allow for more reliable results.

5 Meso-scale Testing

The nanoindentation stresses were in the 10-180 MPa range. The local stresses are therefore very high compared to the usual stresses at which solder joints are submitted in service (1-10 MPa). The aim of the meso-scale testing was to carry out creep tests of entire solder joint at high temperatures in the range of operating stresses (1 to 10 MPa).

5.1 Experimental Procedure

Ceramic BGAs with four SAC305 ($SnAg_{3.0}Cu_{0.5}$) spherical solder joints were manufactured in house. The package comprised of a tape substrate that was bonded with a Cu pad layer in a solder-mask-defined (SMD) configuration. The solder balls were surface mounted onto the Cu pads by means of reflow soldering. The diameter of the pad-solder interface after soldering was estimated at 310 μm. The average grain size determined by Elec-

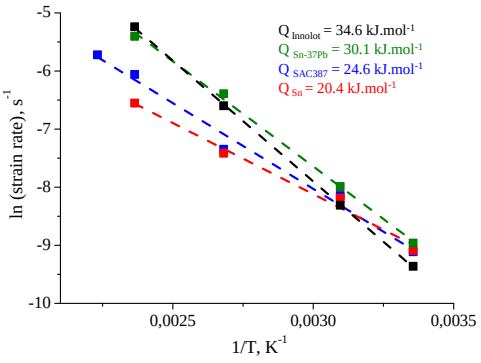

Figure 10: Creep activation energies of SAC387, Sn and Sn-37Pb from elevated temperature nanoindentation creep measurements.

tron Backscattered Diffraction was 11μm (Figure 11). The BGAs were ground on two opposite sides so that the solder connections were ground to half and the assembly was geometrically symmetric. Therefore, shear testing of such BGAs was equivalent to testing two spherical solder joints of 500μm diameter. One side of the BGA was carefully polished (similar procedure than for bulk solders). For microstructural investigation of creep mechanisms, meso-grids were FIBed onto the surface of each solder joint (Figure 12).

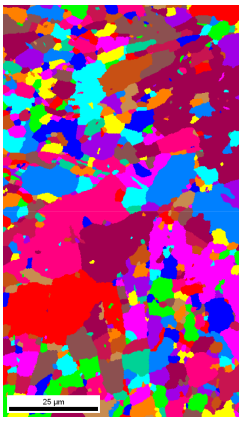

Figure 11: EBSD normal grain orientation map of a CBGA solder joint. Regions of the same orientation are represented with the same colour.

A liquid cell was designed to fit within the NanoTest platform and to carry out high temperature meso-scale tests for BGA electronic assemblies (Figure 13). The liquid cell was filled with low viscosity oil and heated by means of a temperature controller linked to two cartridge heaters and a thermocouple fitted in

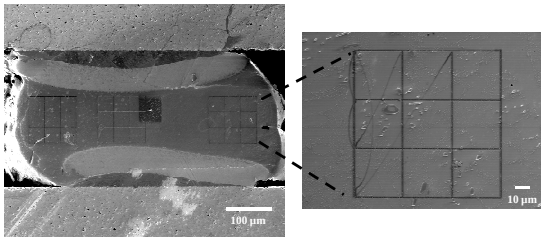

Figure 12: SEM image of meso grids FIBed onto the surface of ceramic BGAs. The lines of the grids were 200nm wide.

slots underneath the cell. A cap covering the cell ensured that minimum heat dissipation occurred. The temperature of the oil was monitored at all times and it was assumed that the temperature of the solder joint was similar to the oil temperature after thermal stabilisation was achieved. Two BGAs and a piece of fused silica (for depth calibration at each temperature) were attached to an aluminium stub by means of a high temperature cement. For each temperature the BGA was shear tested: the upper ceramic board of the BGA was loaded with a spherical stainless steel indenter to 200, 300, 400 and 500 mN. Creep was observed during a 600s dwell time at each of these maximum loads.

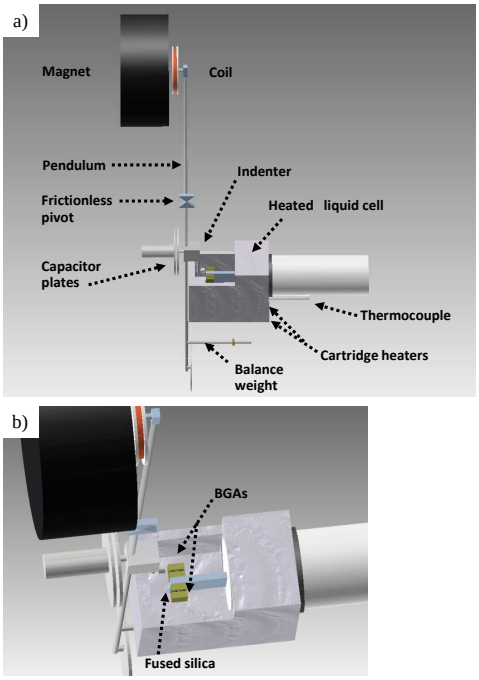

Figure 13: Meso-scale testing platform *a)*Side view; *b)* Interior of the liquid cell

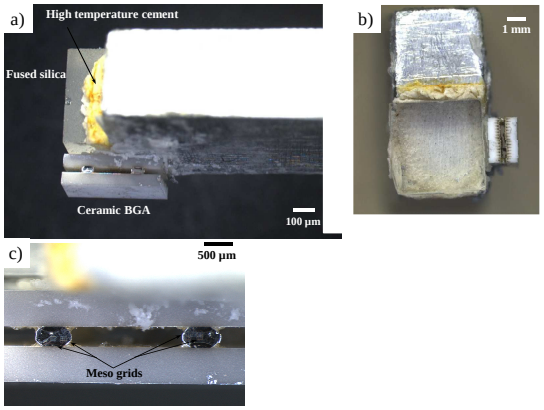

Figure 14: Optical microscopy images of the assembly set-up for testing. *a)* Side view showing the ceramig BGA and the fused silica sample used for depth calibration; *b)* Front view of the set-up and *c*) FIBed mesogrids

5.2 Results and Discussion

The stress range was 1.3< σ <3.3 MPa. Although the set-up is capable of operating to 150°C, preliminary data was only gathered for 25 and 100°C, which gave a strain rate in the range $2.1\text{x}10^{-7} < \dot{\epsilon} < 1.6\text{x}10^{-6}$ s^{-1}. Figure 15 shows that these ranges were similar to literature data for traditional testing methods on SAC alloys. [19] A slight deviation to the hyperbolic sine fit was observed and will be investigated in further work.

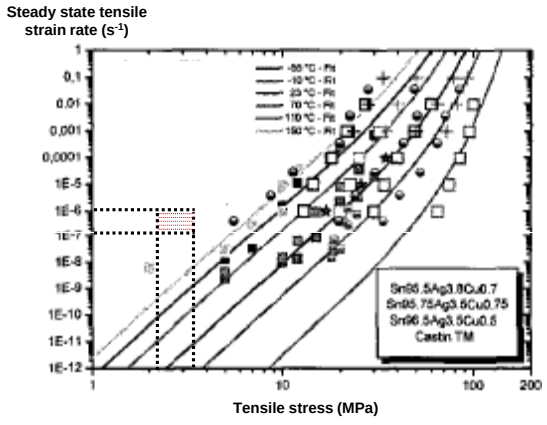

Figure 15: Curve-fitting of SnAgCu creep data to hyperbolic sine model based on 108 data points for various temperatures. [19] The area in red is the zone covered by testing in the 100-500 mN range at 25 and 100°C

Stress exponent values were calculated with the power law. At 25, 50 and 100°C, n was 0.4, 1.8 and 2.0, respectively. The creep activation energy was 16.8 $kJ.mol^{-1}$ for stresses of 2 MPa and 20.6 $kJ.mol^{-1}$ for stresses of 2.6 MPa. These results are slightly lower than literature data (Table 1).

6 Conclusions

- Elevated temperature nanoindentation enabled a first creep characterisation of solder alloys.
- Comparison with literature data showed discrepancies but such discrepancies were observed even amongst similar testing methods, suggesting a high-dependence of creep parameters on processing, geometries and microstructures.
- Promising data was obtained for the mesoscale platform and it is expected that data at higher temperatures will validate the method.

References

[1] Directive 2002/95/ec of the european parliament and of the council of 27 january 2003 on the restriction of the use of certain hazardous substances in electrical and electronic equipment, oj l 37, 13.2.2003, 19.

[2] Espace Hamelin Decision Etudes Conseil. *World Electronic Industries 2008-2013, Executive summary*. 2009.

[3] D. Frear, J. Jang, J. Lin, and C. Zhang. Pb-free solders for flip-chip interconnects. *JOM Journal of the Minerals, Metals and Materials Society*, 53:28–33, 2001.

[4] M. D. Mathew. Creep deformation characteristics of tin and tin-based electronic solder alloys. *Metallurgical and materials transactions.A, Physical metallurgy and materials science*, 36(1):99, 2005.

[5] Xu Chen, Gang Chen, and M. Sakane. Modified anand constitutive model for lead-free solder sn-3.5ag. In *Thermal and Thermomechanical Phenomena in Electronic Systems, 2004. ITHERM '04.*, volume 2, pages 447 – 452, june 2004.

[6] S. Jadhav, T. Bieler, K. Subramanian, and J. Lucas. Stress relaxation behavior of composite and eutectic sn-ag solder joints. *Journal of Electronic Materials*, 30:1197–1205, 2001.

[7] S. N. G. Chu and J. C. M. Li. Impression creep; a new creep test. *Journal of Materials Science*, 12:2200–2208, 1977.

[8] J. Stephens and D. Frear. Time-dependent deformation behavior of near-eutectic 60sn-40pb solder. *Metallurgical and Materials Transactions A*, 30:1301–1313, 1999. 10.1007/s11661-999-0279-2.

[9] T.O. Mulhearn. The deformation of metals by vickers-type pyramidal indenters. *Journal of the Mechanics and Physics of Solids*, 7(2):85 – 88, 1959.

[10] W. C. Oliver. Improved technique for determining hardness and elastic modulus using load and displacement sensing indentation experiments. *Journal of Materials Research*, 7(6):1564, 1992.

[11] R. Goodall and T.W. Clyne. A critical appraisal of the extraction of creep parameters from nanoindentation data obtained at room temperature. *Acta Materialia*, 54(20):5489 – 5499, 2006.

[12] Y.C. Liu, J.W.R. Teo, S.K. Tung, and K.H. Lam. High-temperature creep and hardness of eutectic 80au/20sn solder. *Journal of Alloys and Compounds*, 448(12):340 – 343, 2008.

[13] W. H. Poisl. The relationship between indentation and uniaxial creep in amorphous selenium. *Journal of Materials Research*, 10(8):2024, 1995.

[14] S. Brown. Development of a fatigue resistant lead-free alloy for high relliability under hood applications. *Cookson Electronics Assembly Materials, private communication*, 1990.

[15] T. Chudoba and F. Richter. Investigation of creep behaviour under load during indentation experiments and its influence on hardness and modulus results. *Surface and Coatings Technology*, 148(23):191 – 198, 2001.

[16] M.J. Mayo and W.D. Nix. A micro-indentation study of superplasticity in pb, sn, and sn-38pb. *Acta Metallurgica*, 36(8):2183 – 2192, 1988.

[17] A. Juhasz, P. Tasnadi, P. Szaszvari, and I. Kovacs. Investigation of the superplasticity of tin-lead eutectic by impression creep tests. *Journal of Materials Science*, 21:3287–3291, 1986.

[18] V. Raman. An investigation of creep processes in tin and aluminum using depth-sensing indentation technique. *Journal of Materials Research*, 7(3):627, 1992.

[19] R. Dudek, E. Auerswald, A. Gollhardt, B. Michel, H. Reichl, and A. Schubert. Fatigue life models for snagcu and snpb solder joints evaluated by experiments and simulation. *53rd Electronic Components Technology Conference 2003 Proceedings*, pages 603–610, 2003.

[20] Z. Mei and J. Morris. Characterization of eutectic sn-bi solder joints. *Journal of Electronic Materials*, 21:599–607, 1992.

[21] Characterisation of constitutive behaviour of snag, snagcu and snpb solder in flip chip joints. *Sensors and Actuators A: Physical*, 99(12):188 – 193, 2002.

[22] J. P. Clech. Report to nist on review and analysis of lead-free solder material properties. 2002.

[23] Martin Rist, W. Plumbridge, and S. Cooper. Creep-constitutive behavior of sn-3.8ag-0.7cu solder using an internal stress approach. *Journal of Electronic Materials*, 35:1050–1058, 2006.

[24] Qiang Xiao and William Armstrong. Tensile creep and microstructural characterization of bulk sn3.9ag0.6cu lead-free solder. *Journal of Electronic Materials*, 34:196–211, 2005.

[25] Qian Zhang, A. Dasgupta, and P. Haswell. Viscoplastic constitutive properties and energy-partitioning model of lead-free sn3.9ag0.6cu solder alloy. In *Electronic Components and Technology Conference, 2003. Proceedings. 53rd*, pages 1862 – 1868, 27-30, 2003.

[26] J. Lau. Effects of ramp-time on the thermal-fatigue life of snagcu lead-free solder joints. *Proceedings - Electronic Components Conference*, 55(2):1292, 2005.

[27] John H.L. Pang, B.S. Xiong, and T.H. Low. Low cycle fatigue models for lead-free solders. *Thin Solid Films*, 462463(0):408 – 412, 2004. Proceedings of the International Conference on Materials for Advanced Technologies (ICMAT 2003), Symposium L: Advances in Materials for Si Microelectronics - From Processing to Packaging.

[28] R. Roumina. Room temperature indentation creep of cast pb-sb alloys. *Scripta Materialia*, 51(6):497, 2004.

[29] Fugian Yang and J.C.M. Li. Impression test of 63sn-37pb eutectic alloy. *Materials Science and Engineering: A*, 201(12):40 – 49, 1995.

[30] Q. J. Yang X. Q. Shi, Z. P. Wang and H. L. J. Pang. Creep behavior and deformation mechanism map of sn-pb eutectic solder alloy. *Journal of Engineering Materials and Technology*, 125:81–88, 2003.

Table 1: Measured and published elastic modulus values for Sn, Sn-Pb and SAC alloys. [3,19–27]

Solder alloy	n	Q (kJ.mol^{-1})	Testing method	Reference
Constitutive model: Dorn power law				
Sn	5.8	20.4	Nanoindentation	Own measurements
Sn-40Pb	6.3	20	Lap joint, Shear/Tensile	Mei [20]
Sn-38Pb	1.8		Nanoindentation	Mayo [16]
Sn-37Pb	4.8	30.1	Nanoindentation	Own measurements
Sn-3.5Ag	11	79.8	Flip chip, Tensile	Wiese [21]
	6.05	61.2	Bulk, Tensile	Clech [22]
SAC387	6.3	24.6	Nanoindentation	Own measurements
	3.69	36	Bulk, Tensile	Frear [3]
	7	40	Bulk, Tensile	Rist [23]
SAC405	18	83.1	Flip-chip, Tensile	Wiese [21]
Innolot	8.8	34.6	Nanoindentation	Own measurements
Constitutive model: Garofalo Hyperbolic Sine law				
Sn-40Pb	3.3	52.9	Lap joints, Shear/Tensile	Shi [30]
	3.04	56.9	Bulk, Compression	Frear [3]
Sn-37Pb	1.38	50.0	Bulk, Tensile	Xiao [24]
	2	44.9	Flip-chip joints, Tensile	Wiese [21]
	2.1	54.1	Lap joints, Tensile	Zhang [25]
	3.3	52.8	Bulk, Tensile	Shi [30]
	2.2	59.3	Flip-chip joints, Tensile	Zhang [25]
Sn-3.5Ag	4.75	57.1	Bulk, Tensile	Wiese [21]
	5.04	41.6	Bulk, Tensile	Clech [22]
	8.67	77.4	Lap joints, Shear	Clech [22]
	5.5	72.5	Lap joints, Shear	Clech [22]
	5.5	72.4	Lap joints, Shear	Clech [22]
SAC396	2.89	62.0	Bulk, Tensile	Xiao [24]
	4.2	45	Bulk, Compression	Lau [26]
	3.79	62.3	Lap joints, Tensile	Zhang [25]
	4.0	71.3	Flip-chip joints, Tensile	Pang [27]
SAC387	5.1	65.32	Bulk, Tensile	Pang [27]
	6.41	54.0		Dudek [19]